Unveiling Molecular Changes in Water by Small Luminescent Nanoparticles

*Lucía Labrador-Páez, Dragana J. Jovanovic´, Manuel I. Marqués, Krisjanis Smits, Slobodan D. Dolic´, Francisco Jaque, Harry Eugene Stanley, Miroslav D. Dramic´anin, José García-Solé, Patricia Haro-González, and Daniel Jaque**

***N**owadays a large variety of applications are based on solid nanoparticles dispersed in liquids—so called nanofluids. The interaction between the fluid and the nanoparticles plays a decisive role in the physical properties of the nanofluid. A novel approach based on the nonradiative energy transfer between two small luminescent nanocrystals ($GdVO_4:Nd^{3+}$ and $GdVO_4:Yb^{3+}$) dispersed in water is used in this work to investigate how temperature affects both the processes of interaction between nanoparticles and the effect of the fluid on the nanoparticles. From a systematic analysis of the effect of temperature on the $GdVO_4:Nd^{3+} \rightarrow GdVO_4:Yb^{3+}$ interparticle energy transfer, it can be concluded that a dramatic increase in the energy transfer efficiency occurs for temperatures above 45 °C. This change is properly explained by taking into account a crossover existing in diverse water properties that occurs at about this temperature. The obtained results allow elucidation on the molecular arrangement of water molecules below and above this crossover temperature. In addition, it is observed that an energy transfer process is produced as a result of interparticle collisions that induce irreversible ion exchange between the interacting nanoparticles.*

1. Introduction

Luminescent nanofluids (LNFs) are colloidal suspensions of luminescent nanoparticles (LNPs) in liquid media. LNFs have recently emerged as versatile and powerful tools capable of providing innovative solutions in a wide range of fields, including analytical chemistry, renewable ener-gies, and biomedicine.[1] From a fundamental point of view, LNFs constitute a novel scenario for the study of the physical mechanisms governing interaction processes between nano-particles, and the effect of the solvent on the nanoparticles at the nanoscale level by using the luminescence generated

by LNPs as a tool. For instance, approaches already used to get information on these interaction mechanisms involve the study of the Brownian colloidal nature of LNFs due to the interaction of the molecules of the fluid with the LNPs,[2] radiation trapping between LNPs,[3] the enhancement of the stability of the luminescence of silica nanocrystals,[4] or even efficient nonradiative energy transfer processes between LNPs in close proximity.[5] The physics of LNFs is even more mysterious and challenging when dealing with colloidal small (≈3 nm) luminescent nanoparticles (SLNPs). In such small NP sizes, over 80% of constituent atoms are located on the surface. Therefore, an enormous fraction of the constituent atoms is in physical contact with the solvent molecules or with other SLNPs. As a consequence, any change in the envi-ronment of an SLNP or even the interparticle interactions affects most of their atoms, and thus has a major impact on their luminescent properties. Thus, we expect that a thorough analysis of the luminescence generated by LNFs containing SLNPs will provide information about both the molecular status of the liquid solvent and the nature and magnitude of interaction events between SLNPs.

The use of LNFs for nanoscale molecular investiga-tions is especially exciting when applied to water—the most common substance on earth and indispensable in life and human development. Although water has been studied for decades and most of its properties are well known, the inter-actions between water molecules are not fully understood. In particular, thermal anomalies in liquid water properties are still a matter of debate.[6] Indeed most water proper-ties have been studied by macroscopic techniques, such as optical and dielectric spectroscopy, and they do not provide details at the molecular level. Questions about the molecular dynamics of water remain unanswered, such as a crossover at around 45 °C that affects a large variety of water properties and the thermal stability of biological macromolecule as pro-teins.[7] As this anomaly takes place within the physiological temperature range, it is expected to have a great impact in the use of nanofluids for biomedical applications.[8] The use of nanoscopic techniques capable of monitoring dynamic molecular interactions at the molecular scale will enable us to better understand the dynamics of water, the use of LNFs containing SLNPs in particular.

The goal of this work is to understand the crossover in the molecular behavior of water at ≈45 °C by means of inter-particle energy transfer (IPET) between two different kind of SLNPs (donor and acceptor SLNPs), both coexisting in the same LNF.[9] As previously reported by Sarkar et al.,[9b] after the optical excitation of donor SLNPs, energy transfer to the acceptor SLNPs may occur via collision-assisted processes caused by the thermal motion of both donor and acceptor SLNPs in the solvent fluid.[2] Thus energy transfer in colli-sion-assisted IPET (CA-IPET) takes place when the donor and acceptor SLNPs collide, such that the superficial lumi-nescent ions of the interacting SLNPs are in a distance range allowing nonradiative energy transfer. CA-IPET efficiency ($\varphi_{CA\text{-}IPET}$) is strongly correlated with the molecular struc-ture of the solvent and, consequently, temperature-induced changes in the water molecular properties will strongly affect

2. Results and Discussion

The used SLNPs consist of $GdVO_4$ small nanocrystals doped with either Nd^{3+} (donor nanoparticles) or Yb^{3+} ions (acceptor nanoparticles), hereafter designated SLNPs:Nd and SLNPs:Yb, respectively. Trivalent rare-earth-ion-doped SLNPs are excellent optical probes and display narrow absorption and emission bands.[10] In addition, the energy levels of both Nd^{3+} and Yb^{3+} lead to a phonon-assisted spectral overlap between the emission of Nd^{3+} ions and the absorption of Yb^{3+} ions, which ensures the possibility of an efficient $Nd^{3+} \rightarrow Yb^{3+}$ nonradiative energy transfer when the SLNPs:Nd and SLNPs:Yb are close to each other.[11] Details about synthesis procedure and morphological properties of these SLNPs are supplied in the Experimental Section and in Sections S1 and S2 (Supporting Information). **Figure 1**a,b shows that the average diameter of both SLNPs:Nd and SLNPs:Yb is $D_{NP} = 2.9 \pm 0.5$ nm. Figure 1a shows a trans-mission electron microscopy (TEM) image revealing that the crystallographic structure is preserved even at small sizes. Figure 1c shows digital pictures of the SLNPs:Nd and SLNPs:Yb LNFs, which were prepared separately in stable colloidal aqueous suspensions. Figure 1e displays a digital picture of LNF containing both SLNPs:Nd and SLNPs:Yb, which was obtained by mixing certain volumes of the original suspensions. Both original and mixed LNFs are colloidal, and even over a period of months do not precipitate. Figure 1d shows a room temperature emission spectra generated by the original (unmixed) LNFs under 808-nm laser excitation, i.e., under a selective excitation of Nd^{3+} ions (see the absorp-tion of LNFs in Figure S7 in the Supporting Information). As expected, no luminescence is generated by the LNF containing only SLNPs:Yb (see also Figure S8 in the Sup-porting Information). On the other hand, the emission spec-trum generated by the LNFs containing only SLNPs:Nd in the studied spectral range (950–1125 nm) is the well-known $^4F_{3/2} \rightarrow {}^4I_{11/2}$ infrared emission band of Nd^{3+} ions centered at ≈1060 nm. Taking into account the energy level diagrams of Nd^{3+} and Yb^{3+} ions (shown schematically in Figure 1c,e), only SLNPs:Nd generate luminescence under 808-nm excitation (which matches the $^4I_{9/2} \rightarrow {}^4F_{5/2}$ absorption band of Nd^{3+} ions). Figure 1f shows the emission spectra (optically excited by 808-nm laser light) obtained at different temperatures when the LNF contains both SLNPs:Nd and SLNPs:Yb. All display the 1060-nm emission band of Nd^{3+} and the characteristic emission band of Yb^{3+} centered at 980 nm ($^2F_{5/2} \rightarrow {}^2F_{7/2}$ transi-tion), revealing that $Nd^{3+} \rightarrow Yb^{3+}$ energy transfer takes place, i.e., the IPET process. In this IPET process, SLNPs:Nd are donor units that absorb 808 nm of excitation energy and par-tially transfer energy to the SLNPs:Yb acceptor units. Note that for close to ambient temperatures (20–30 °C in Figure 1f) we see only weak traces of Yb^{3+} ion emission, but when tem-peratures exceed 45 °C (80 °C in Figure 1f) we observe a substantial increase in the Yb^{3+} ions emission and a corre-sponding decrease in the emission of Nd^{3+} ions, which indi-cates a strong increase in the IPET. The nonradiative nature of this IPET process has been confirmed by the shortening of the emission lifetime of the donor ion (Nd^{3+}) in the presence of SLNPs:Yb (see Section S3 in the Supporting Information).

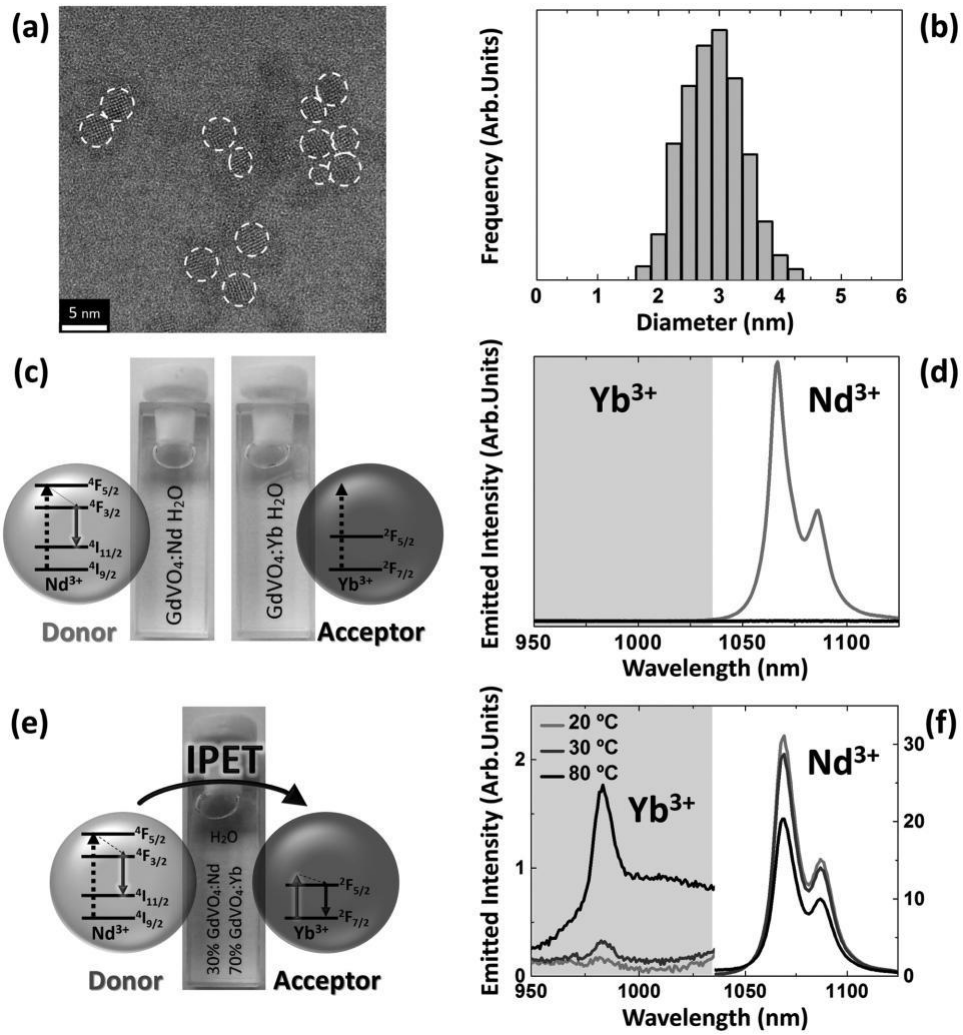

Figure 1. Characterization of the SLNPs and emission of the LNFs. a) TEM image of a mix of SLNP:Nd and SLNP:Yb (dashed circles show the positions of the SLNPs). b) Size distribution obtained from the analysis of TEM images. c) Schematic representation of the energy levels of Nd^{3+} and Yb^{3+} ions accounting for the emission (dotted arrow) obtained under selective excitation of Nd^{3+} ions (808 nm; gray arrow) and optical image of the cuvettes containing the LNFs with either SLNP:Nd or SLNP:Yb. d) Emission spectra of the LNFs shown in (c). e) Schematic representation of the energy levels of Nd^{3+} and Yb^{3+} ions accounting for the emissions (gray arrow Nd^{3+} and black arrow Yb^{3+}) obtained from the mixed LNF under optical excitation of Nd^{3+} ions (dotted arrow) and the IPET process (an optical image of the cuvette containing the mixed LNF is also shown). f) Emission spectra of this LNF at three different temperatures.

Thus the data in Figure 1 evidence the presence of IPET in LNFs containing both SLNPs:Nd and SLNPs:Yb, but it does not reveal the responsible mechanism. The litera-ture indicates two possible mechanisms that could explain IPET. The first one is the well-known Dexter–Förster IPET (DF-IPET) that assumes that electric dipole interaction causes noncontact energy transfer between donor and acceptor units. The second one is the CA-IPET described above,[9b] in which the IPET from donor to acceptor particles occurs when they collide. As explained in Section S4 (Sup-porting Information), we can discriminate between DF-IPET and CA-IPET by studying the dependence of $\varphi_{CA\text{-}IPET}$ on fluid viscosity (η). An increase in η reduces the collision rate, and thus $\varphi_{CA\text{-}IPET}$, for a CA-IPET process. On the other hand, η does not affect φ_{IPET} for a dominant DF-IPET pro-cess. **Figure 2**a shows the emission spectra obtained from mixed LNFs of different η that preserve the same average interparticle distances. The procedure for controlling the η variation is described in the Experimental Section. Figure 2b shows how $\varphi_{CA\text{-}IPET}$ decreases as the solvent fluid η increases. We also obtain a $\varphi_{CA\text{-}IPET} \propto 1/\eta$ trend, identical to that expected for a pure CA-IPET process (see Section S4 in the Supporting Information). We thus conclude that collisions are the dominant mechanism leading to the interparticle energy transfer in the mixed LNF.

Figure 3a shows the dependence of $\varphi_{CA-IPET}$ on the LNF temperature in the 20–80 °C range obtained during a heating and cooling cycle. Two regimes are observed during the heating process. In the 10–40 °C range, the $\varphi_{CA\text{-}IPET}$ increases linearly with temperature at a rate of $d\varphi_{CA\text{-}IPET}/dT \approx 0.45\%\ °C^{-1}$. In the 60–80 °C range, $\varphi_{CA\text{-}IPET}$ increases linearly with temperature but with a much larger rate of $d\varphi_{CA\text{-}IPET}/dT \approx 3.2\%\ °C^{-1}$. Note that these two regimes cannot be correlated to morphological changes affecting the

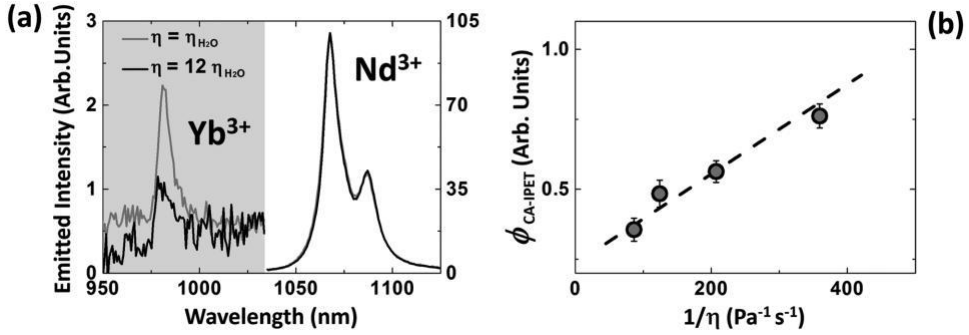

Figure 2. Dependence of IPET efficiency on viscosity. a) Emission spectra of the mixed LNF under optical excitation at 808 nm (i.e., optical excitation of doped SLNP:Nd) as obtained for two different viscosities of the solvent. b) Dependence of the CA-IPET efficiency on the inverse of fluid viscosity η. Symbols are experimental data and dashed line is a guide for the eyes.

SLNPs caused by, e.g., particle agglomeration or temperature-induced Ostwald ripening. Figure 3b shows SLNPs average size from TEM experiments conducted on the mixed LNF at different temperatures (see Figure S3 in the Supporting Information), confirming that within the error bars the size of the SLNPs remains unchanged. The two trends observed in the $\varphi_{\text{CA-IPET}}$ versus temperature experiment may reveal the existence of a crossover in the molecular structure of water at H45 °C, which would modify the dynamics of interparticle collisions and change the dependence of $\varphi_{\text{CA-IPET}}$ on temperature. Note also that the molecular structure of water at temperatures below 45 °C minimizes the interaction between SLNPs, which makes $\varphi_{\text{CA-IPET}}$ weakly dependent on temperature in this range. As mentioned above, the existence of this 45 °C water crossover was reported in several studies of the optical, mechanical, and dielectric properties of water.[7] We will relate this anomaly to the temperature-induced dissocia-tion of water molecules clusters later in this report.

Figure 3a shows that although $\varphi_{\text{CA-IPET}}$ increases by more than one order of magnitude when subjected to a heating cycle, it remains temperature independent when cooled. This nonreversibility is not due to a CA-IPET process, in which the SLNPs involved in the collision events should not be altered. Clearly, the collision events permanently modify the SLNPs somehow. Figure 3b shows TEM results that rule out structural and morphological changes in the nanoparticles after collision events. Therefore the observed spectral hys-teresis may be due to interparticle ion exchange during col-lision events. Figure 3c shows a schematic representation of the ion-exchange mechanism. When an SLNP:Nd and an SLNP:Yb collide, during the time interval of physical contact the SLNPs exchange superficial atoms, Nd^{3+} and Yb^{3+} ions

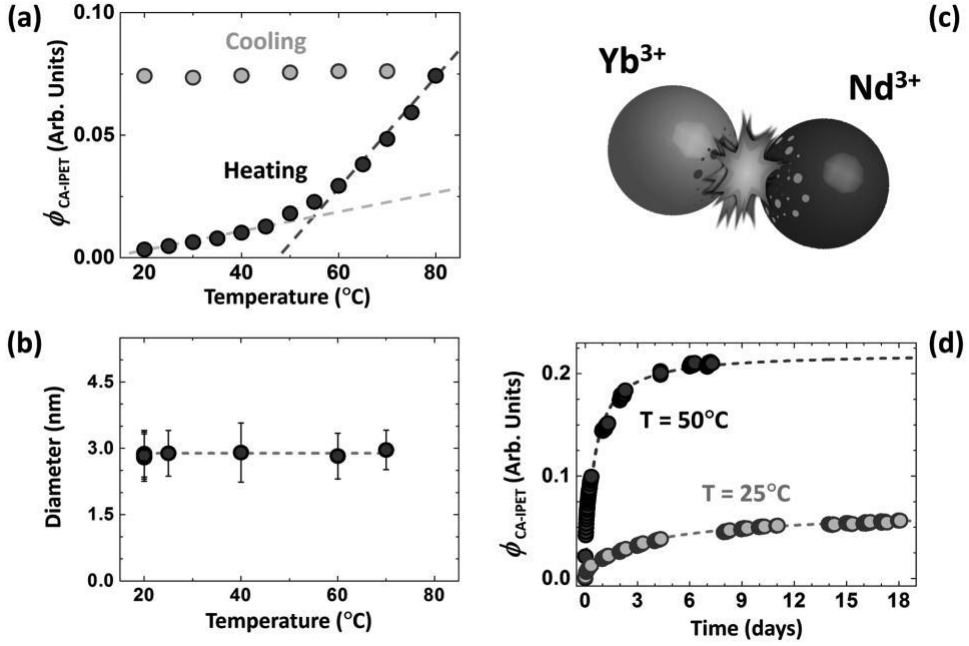

Figure 3. Dependence of IPET efficiency on temperature. a) Temperature dependence of the CA-IPET efficiency as obtained during a heating (black) and cooling (gray) cycle. Dashed lines are guides to the eyes in order to make evident the existence of two distinguished regimes. b) Diameter of the SLNPs estimated from TEM images of mixed LNF heated at diverse temperatures. c) Schematic representation of a collision-assisted interparticle ion exchange process. d) Long-term evolution of CA-IPET efficiency as obtained at two different temperatures (25 °C (gray) and 50 °C (black)). Symbols are experimental data and dashed lines are guides to the eyes.

among them, and a fraction of Yb^{3+} (Nd^{3+}) ions are incorporated on the surface of the SLNP:Nd (SLNP:Yb). After this collision-assisted ion exchange occurs, the distance between Nd^{3+} (donor) and Yb^{3+} (acceptor) ions is on the order of the SLNP size (2.9 nm), much lower than the average distance between SLNPs in the LNF (≈10 nm), which was the distance between ions initially. Due to the fact that the distance between donor and acceptor ions is significantly reduced after the ion exchange, $\varphi_{CA\text{-}IPET}$ increases. This explains the maximum value of $\varphi_{CA\text{-}IPET}$ experimentally obtained after the heating and cooling cycle. In addition, once ion exchange has occurred, no further collisions are needed for the efficient energy transfer. Thus the lower collision rate (the lower temperature) during the cooling procedure does not lower $\varphi_{CA\text{-}IPET}$.

To experimentally verify the presence of interparticle ion exchange in the LNFs, we keep their temperature constant and measure the long-term evolution of $\varphi_{CA\text{-}IPET}$. Note that at any given temperature collisions between SLNPs happen at a given rate that is proportional to this temperature. Thus ion exchange is occurring, and the $\varphi_{CA\text{-}IPET}$ increases with time until it reaches saturation. The time needed to reach saturation is strongly temperature dependent. Higher temperatures increase collision rates, speed up the ion exchange process, and shorten the time to saturation. Figure 3d shows the long-term evolution of $\varphi_{CA\text{-}IPET}$ at 25 and 50 °C for a mixed LNF. As predicted for the CA-IPET process in the presence of ion exchange, experimentally we find saturation dynamics at both temperatures and a shorter saturation time at the higher temperature. Figure 3d and Figure S9 (Supporting Information) also reveal that a more efficient interparticle ion exchange is produced at higher temperatures, as higher $\varphi_{CA\text{-}IPET}$ values, together with a corresponding important shortening of the lifetime of the donor ions, are observed after long-term evolution at 50 °C. X-ray diffraction measurements and TEM images of the LNF after these experiments (Figures S2 and S4 and Table S1, Supporting Information) confirm that the LNP has not suffered significant morphological modifications during long-term evolution. Figure 3d shows experimental data indicating that the changes in the luminescent properties of the mixed LNF can only be understood in terms of a synergy between interparticle collisions and ion exchange events. Note that we assume that ion exchange occurs in a colloidal suspension of LNPs. This has also been reported by several researchers, although they did not correlate it with interparticle collisions.[12] The effect of the long-term evolution at diverse temperatures (i.e., ion exchange saturation in the two regimes of water) on the temperature dependence of the $\varphi_{CA\text{-}IPET}$ is studied in Section S5 (Supporting Information).

Figures 2 and 3 show experimental data that we now analyze using a simple model in order to correlate the temperature dependence of $\varphi_{CA\text{-}IPET}$ with a crossover in the molecular behavior of water at ≈45 °C. For short time periods and far from saturation, the transfer efficiency ($\varphi_{CA\text{-}IPET}$) at a given temperature (T_i) is:

$$\varphi_{CA\text{-}IPET}(T_i) = \varphi_{CA\text{-}IPET}(T_{i-1}) + \varphi(T_i)\,\Delta t \quad (1)$$

where t is the measurement lap time at each T (where T_{i-1} is the previous measured temperature), and φ is the total number of successful collisions between LNPs (i.e., collisions leading to ion exchange) per unit time. The successful collisions are quantified by multiplying the total number of collisions per unit time by the probability of obtaining ion transfer (κ) and the probability that there is energy transfer between ions (W). Because the total number of collisions per unit time is proportional to the temperature-dependent diffusion constant (D), the proportionality expression for κ is:

$$\kappa(T_i) \propto \frac{\phi_{CA\text{-}IPET}(T_i) - \phi_{CA\text{-}IPET}(T_{i-1})}{D(T_i)W(T_i)} \quad (2)$$

The diffusion constant is given by $D = k_B T/(3\pi\eta D_{NP})$, where k_B is the Boltzmann constant. Knowing the temperature dependence of W and η (see the data in Section S6 in the Supporting Information), we can determine the temperature dependence of κ from the experimental data shown in Figure 3a. **Figure 4**a shows the temperature dependence of κ, which remains approximately constant below 45 °C and is thermally activated at higher temperatures, growing according to logarithmic dependence on the inverse of the absolute temperature. The low $\varphi_{CA\text{-}IPET}$ values below 45 °C are caused by the formation of water molecule cages around the SLNPs that fluctuate in time, impede collisions, and inhibit ion exchange. These cages disappear when temperature increases and therefore the collision-assisted ion exchange is thermally activated.[7d] The insets in Figure 4d schematically show both situations.

The temperature-induced dissociation of water cages around the SLNPs indicates that, as previously proposed,[7] there is a crossover between the regular water state and a hydrogen-bonded state. We now further explore the existence of this crossover by examining the dielectric behavior of liquid water to quantify at each temperature the value of i) the dipole moment and ii) the associated critical temperature (T_C) in terms of Curie–Weiss behavior.[13] Figure 4b,c shows the results for (i) and (ii), respectively. Note how the dipole moment value falls between the accepted gas and ice values for the water molecule (1.84D and 2.6D, respectively), and how liquid water is always in the paraelectric phase. Since the value of the dipole moment of the water molecule is dependent upon the average number of clustered water molecules,[14] the average number of water molecules in each cluster at a given temperature (i.e., the number of water molecules able to interact between them to form cages) shown in Figure 4d is determined from the temperature dependence of the dipole moment shown in Figure 4b. Note that, for temperatures above ≈45 °C, the existence of pairs of hydrogen-bonded water molecules starts to be unlikely, and this implies a decrease in the stability of the hydrogen bonded clusters surrounding the LNPs. This explains the disappearance of the rates, and the temperature dependence of $\varphi_{CA\text{-}IPET}$ shown in Figure 3a.

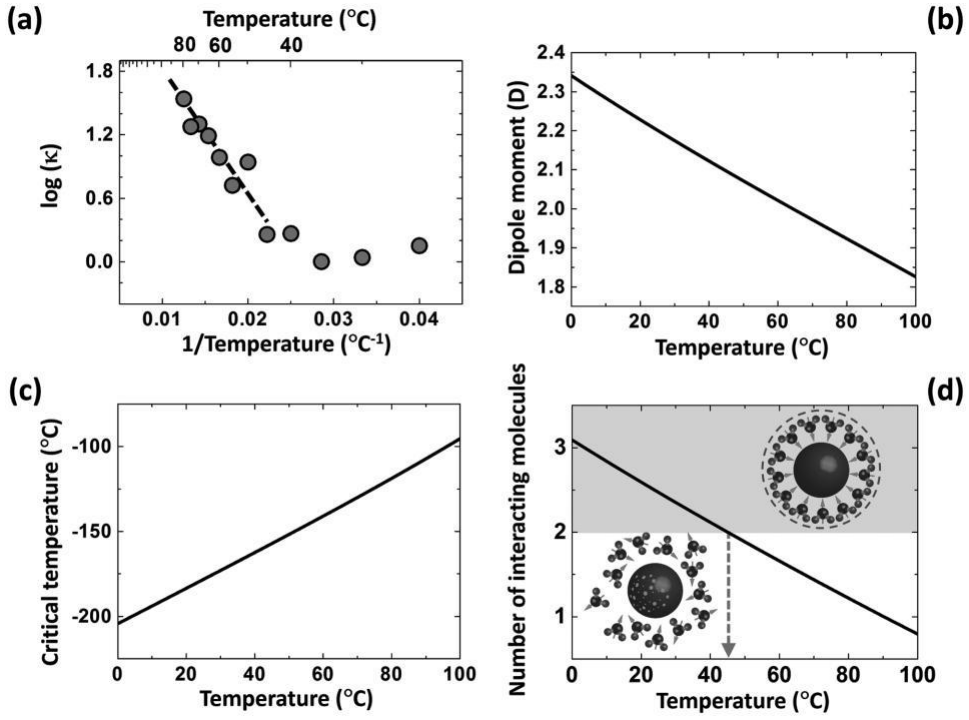

Figure 4. Crossover between water molecular behaviors. a) Logarithm of the ion transfer probability (except for a temperature independent constant) as a function of the inverse of temperature. A 1/*T* linear dependence is only experimentally found for temperatures above 45 °C (dashed line). b) Dipole moment of water and c) critical temperature T_C (also known as Curie temperature) estimated from dielectric data as a function of temperature. d) Number of interacting molecules in water as a function of temperature. Insets: Schematic diagram of water molecules (top) interacting between them and so forming a cage that inhibits collisions and (bottom) being unable to interact among them and so allowing for interparticle collisions. Dashed arrow points out the crossover temperature.

3. Conclusion

In summary, we have used small luminescent nanoparticles doped with different rare earth ions as colloidal donor and acceptor units to study the interparticle energy transfer pro-cess in water-based nanofluids. We have found that there is interparticle energy transfer between colloidal small lumi-nescent nanoparticles. This process is mediated by inter-particle collisions, which increase the rate of nonreversible exchange of the luminescent ions between nanoparticles. The experimental data show that the interparticle energy transfer efficiency displays an unusual temperature depend-ence: A weak trend is observed below 45 °C and strong one above this temperature. This unusual temperature-dependent behavior indicates that there is a change in the molecular behavior of water at this temperature that is due to the exist-ence of a diffuse crossover at H45 °C between a hydrogen-bonded and a regular state of water.

This indicates that the molecular structure of the solvent plays a decisive role in the interparticle dynamics of nano-fluids. In addition, the optical spectroscopy of colloidal small luminescent nanoparticles is a powerful tool in the study of molecular interactions of liquids. Therefore, the results pre-sented in this work open new avenues in which small lumi-nescent nanoparticles can be used as local molecular probes to study the molecular interactions of not just water but also a variety of other liquids.

4. Experimental Section

Reagents and Synthesis: Ammonium metavanadate (NH_4VO_3; min. 99.0%, Alfa Aesar), trisodium citrate dihydrate ($Na_3C_6H_5O_7$; 99+%, Sigma-Aldrich), gadolinium(III) nitrate hexahydrate ($Gd(NO_3)_3 \times 6H_2O$; 99.9%, Alfa Aesar), neodymium(III) nitrate hex-ahydrate ($Nd(NO_3)_3 \times 6H_2O$; 99.9%, Alfa Aesar), and ytterbium(III) nitrate pentahydrate ($Yb(NO_3)_3 \times 5H_2O$; 99.9%, Alfa Aesar) were used without further purification. Milli-Q deionized water (electrical resistivity = 18.2 MΩ cm^{-1}) was utilized as a solvent. Spectra/Por 3 dialysis membrane, Standard RC Tubing, MWCO: 3.5 (Spectrum Laboratories, Inc.) was used for the dialysis of prepared colloidal suspensions. Colloidal suspensions of Nd^{3+} and Yb^{3+} doped $GdVO_4$ SLNPs were prepared by following the procedure which is described in a recent paper.[15] A detailed description of the procedure is included in Section S1 (Supporting Information).

General Conditions for Structural Characterization: Samples for structural characterization were obtained by evaporation of aqueous colloidal solutions. X-ray diffraction measurements were performed with Rigaku SmartLab diffractometer using CuKα1.2 radiation (λ = 0.15405 nm). Diffraction data were recorded with a step of 0.01° and a counting time of 1° min^{-1} over the 2θ range from 10° to 100°. The study of particle morphology was accom-plished using transmission electron microscope Tecnai G2 F20 (FEI) operated at 200 kV. The samples for TEM studies were placed on an ultrathin carbon film (3 nm) mounted on top of a supporting carbon holey film S187-4 (agar Scientific).

General Conditions for Optical Characterization: Emission measurements were performed under excitation at 808 nm by means of a single-mode fiber-coupled laser diode. Laser light was collimated using a fiber port and focused through a 20× NA = 0.4 microscope objective, that at the same time collects the lumines-cence of the NPs. Emission and excitation light were discriminated by means of a wavelength selective mirror and a 830-nm long-pass filter. Finally, the luminescence of the LNPs was analyzed by a spec-trometer (Andor, Oxford Instruments) and recorded by an InGaAs detector. The temperature of the LNFs was controlled by employing a heating plate with an uncertainty of 0.1 °C. The temperature was increased/decreased at a maximum rate of 2.5 °C min^{-1}. In order to guarantee the homogeneous heat distribution in the cuvette containing the sample, a thermal stabilization time of 15 min was hold before each measurement. A thermal gradient in the cuvette of less than 1 °C was achieved. The intensity decay curves of the luminescence of the donor ions in LNFs were obtained by exciting the LNFs at 808 nm using an optical parametric oscillator source (Spectra Physics). The light emitted by the LNFs was spectrally ana-lyzed by means of a spectrometer and then the intensity decay at 892 nm. $^4F_{3/2} \rightarrow {}^4I_{9/2}$ transition was measured by using a photo-multiplier tube (R636-10, Hamamatsu) and a digital oscilloscope (LT372, LeCroy). Notice that this allows to measure the decay time of the $^4F_{3/2}$, excited state which is also the one responsible for the 1060-nm emission.

General Procedure for Controlled Variation of Viscosity and Viscosity Estimation: Small controlled amounts of soap (Liquinox, Alconox) (with a viscosity of ≈500 mPa s) were added to the LNF up to a volume 2.3% of the total volume of the LNF. The density of LNPs in the LNF was varied through this process by no more than a 2.3%, which means that the average distance between LNPs was only increased up to 0.09 nm. These variations are not significant in terms of spectral modifications.

Acknowledgements

This work was supported by the Spanish Ministerio de Educación y Ciencia (MAT2013-47395-C4-1-R and MAT2016-75362-C3-1-R) and by the COST Action CM1403. L.L.-P. thanks the Universidad Autónoma de Madrid for the "Formación de Personal Investi-gador (FPI-UAM)" program. P.H.-G. thanks the Spanish Ministerio de Economia y Competitividad (MINECO) for the Juan de la Cierva program. The authors from the University of Belgrade acknowl-edge the financial support of the Ministry of Education, Science and Technological Development of the Republic of Serbia (Project Nos. 45020 and 172056). M.I.M. thanks financial support from the Spanish Ministerio de Economía y Competitividad (MICINN) Project FIS2015-69295-C3-3-P and the "María de Maeztu" Program Ref: MDM-2014-0377. The work of K.S. was supported by the Latvian National Research Program IMIS2 (Grant No. 302/2012).

[1] a) W. Yu, H. Xie, *J. Nanomater.* **2012**, *2012*, 1; b) O. Mahian, A. Kianifar, S. A. Kalogirou, I. Pop, S. Wongwises, *Int. J. Heat Mass Transfer* **2013**, *57*, 582; c) L. Zhang, Y. Jiang, Y. Ding, M. Povey, D. York, *J. Nanopart. Res.* **2007**, *9*, 479.

[2] C. D. Brites, X. Xie, M. L. Debasu, X. Qin, R. Chen, W. Huang, J. Rocha, X. Liu, L. D. Carlos, *Nat. Nanotechnol.* **2016**, *11*, 851.

[3] P. Rodríguez-Sevilla, H. Rodríguez-Rodríguez, M. Pedroni, A. Speghini, M. Bettinelli, J. G. Solé, D. Jaque, P. Haro-González, *Nano Lett.* **2015**, *15*, 5068.

[4] J. B. Miller, N. Dandu, K. A. Velizhanin, R. J. Anthony, U. R. Kortshagen, D. M. Kroll, S. Kilina, E. K. Hobbie, *ACS Nano* **2015**, *9*, 9772.

[5] A. Bednarkiewicz, M. Nyk, M. Samoc, W. Strek, *J. Phys. Chem. C* **2010**, *114*, 17535.

[6] a) P. Gallo, K. Amann-Winkel, C. A. Angell, M. A. Anisimov, F. D. R. Caupin, C. Chakravarty, E. Lascaris, T. Loerting, A. Z. Panagiotopoulos, J. Russo, *Chem. Rev.* **2016**, *116*, 7463; b) A. Nilsson, L. G. Pettersson, *Nat. Commun.* **2015**, *6*, 8998.

[7] a) L. Maestro, M. Marqués, E. Camarillo, D. Jaque, J. G. Solé, J. Gonzalo, F. Jaque, J. C. D. Valle, F. Mallamace, H. Stanley, *Int. J. Nanotechnol.* **2016**, *13*, 667; b) J. C. del Valle, E. Camarillo, L. Martinez Maestro, J. A. Gonzalo, C. Aragó, M. Marqués, D. Jaque, G. Lifante, J. G. Solé, K. Santacruz-Gómez, *Philos. Mag.* **2015**, *95*, 683; c) F. Mallamace, C. Corsaro, H. E. Stanley, *Sci. Rep.* **2012**, *2*, 993; d) J. G. Davis, K. P. Gierszal, P. Wang, D. Ben-Amotz, *Nature* **2012**, *491*, 582.

[8] a) J. Shi, P. W. Kantoff, R. Wooster, O. C. Farokhzad, *Nat. Rev. Cancer* **2017**, *17*, 20; b) D. Jaque, L. M. Maestro, B. Del Rosal, P.Haro-Gonzalez, A. Benayas, J. Plaza, E. M. Rodriguez, J. G. Sole, *Nanoscale* **2014**, *6*, 9494.

[9] a) F. Wang, R. Deng, J. Wang, Q. Wang, Y. Han, H. Zhu, X. Chen, X. Liu, *Nat. Mater.* **2011**, *10*, 968; b) S. Sarkar, B. Meesaragandla, C. Hazra, V. Mahalingam, *Adv. Mater.* **2013**, *25*, 856.

[10] S. Hao, G. Chen, C. Yang, *Theranostics* **2013**, *3*, 331.

[11] D. Jaque, M. Ramirez, L. Bausa, J. G. Solé, E. Cavalli, A. Speghini, M. Bettinelli, *Phys. Rev. B* **2003**, *68*, 035118.

[12] a) S. Han, X. Qin, Z. An, Y. Zhu, L. Liang, Y. Han, W. Huang, X. Liu, *Nat. Commun.* **2016**, *7*, 13059; b) M. Deng, L. Wang, *Nano Res.* **2014**, *7*, 782; c) C. Dong, F. C. van Veggel, *ACS Nano* **2008**, *3*, 123.

[13] C. Malmberg, A. Maryott, *J. Res. Natl. Bur. Stand.* **1956**, *56*, 1.

[14] J. Gregory, D. Clary, K. Liu, M. Brown, R. Saykally, *Science* **1997**, *275*, 814.

[15] B. del Rosal, A. Pérez-Delgado, M. Misiak, A. Bednarkiewicz, A. S. Vanetsev, Y. Orlovskii, D. J. Jovanovic´, M. D. Dramic´anin, U. Rocha, K. U. Kumar, *J. Appl. Phys.* **2015**, *118*, 143104.

Institute of Solid State Physics, University of Latvia as the Center of Excellence has received funding from the European Union's Horizon 2020 Framework Programme H2020-WIDESPREAD-01-2016-2017-TeamingPhase2 under grant agreement No. 739508, project CAMART²